

Band-modulation of MgZnO/ZnO Metal-semiconductor-metal Photodetectors

Jundar Hwang¹, and Junshou Lin¹

¹Department of Electrophysics, National Chiayi University, Chiayi, Taiwan, China.

Abstract. Magnesium (Mg) diffusion behavior on the band modulation of Mg_xZn_{1-x}O/ZnO metal-semiconductor-metal photodetectors (MSM-PDs) was studied. As the annealing temperature increases, Mg atoms diffuse from Mg_xZn_{1-x}O into the underlying ZnO layer, which modulates the detection band of the fabricated MSM-PDs from two distinct bands into one band. For the annealing temperature lower than 900 °C, two detection bands were achieved located in the wavelength region of 280–320 nm and 360–400 nm, attributed to the absorption of the Mg_xZn_{1-x}O and the ZnO layer, respectively. When the annealing temperature is raised to 900 °C, the Mg_xZn_{1-x}O/ZnO bi-layer becomes homogenized into a single Mg_xZn_{1-x}O layer, leading to only one detection band with a wavelength region of 280–340 nm. In the photoluminescence measurement, the as-deposited Mg_xZn_{1-x}O/ZnO bi-layer demonstrates two distinct emission peaks located at about 340 and 400 nm for the absorption of the Mg_xZn_{1-x}O and ZnO layers, whereas only one emission peak of 355 nm was observed in the 900 °C-annealed Mg_xZn_{1-x}O/ZnO bi-layer.

1 Introduction

ZnO and Mg_xZn_{1-x}O-based ultraviolet (UV) photodetectors (PDs) have been continuously studied because the ZnO material has many advantages, including a wide band gap (3.37 eV), high transparency (>80%) in the visible wavelength region, high exciton binding energy (60 meV), and non-toxicity [1,8]. By mixing ZnO with another wide-direct-band-gap material, MgO (7.8 eV), the tunable bandgap material of Mg_xZn_{1-x}O, which can modulate the detection wavelength of PDs by varying Mg content, can be formed [9-11]. In addition, no significant lattice distortion is found in the Mg_xZn_{1-x}O material because Mg⁺² has a very similar ionic radius to that of Zn⁺² [12].

Although GaN and Al_xGa_{1-x}N materials have been employed in various PDs, expensive and high-temperature technology was required to grow the GaN and Al_xGa_{1-x}N materials, including molecular beam epitaxy and metal organic chemical vapor deposition systems. In contrast, ZnO and Mg_xZn_{1-x}O materials can be grown using low-cost and low-temperature techniques, including radio-frequency (RF) magnetron sputtering and hydrothermal methods [13,14]. As opposed to pure ZnO or Mg_xZn_{1-x}O materials, the

· Corresponding author: jundar@mail.ncyu.edu.tw

$\text{Mg}_x\text{Zn}_{1-x}\text{O}/\text{ZnO}$ bi-layer heterostructure is a promising technological platform as evidenced heterojunction field-effect transistor, multi-quantum-well (MQW) light-emitting diodes, MQW-PDs, and optoelectronic devices with superlattice, as well as two-dimensional electron gas (2DEG) structures [15].

Previously, many $\text{Mg}_x\text{Zn}_{1-x}\text{O}/\text{ZnO}$ heterojunction UV-PDs were fabricated [16-120]. As compared to the MSM-PDs without the $\text{Mg}_x\text{Zn}_{1-x}\text{O}$ capping layer, the PDs with the $\text{Mg}_x\text{Zn}_{1-x}\text{O}/\text{ZnO}$ bi-layer presented higher dark current, photocurrent, and photoresponsivity due to the shielding of ambient oxygen, defect, and surface states passivation by the $\text{Mg}_x\text{Zn}_{1-x}\text{O}$ capping layer [21]. The $\text{Au}/\text{Mg}_x\text{Zn}_{1-x}\text{O}/\text{ZnO}$ PDs had larger responsivity than $\text{Au}/\text{ZnO}/\text{Mg}_x\text{Zn}_{1-x}\text{O}$ PDs [22]. By varying the applied bias voltage, the detection wavelength of the $\text{Mg}_x\text{Zn}_{1-x}\text{O}/\text{ZnO}$ MSM-PDs could be modulated from a single to a dual wavelength [23]. MgZnO/ZnO bi-layer with 2DEG behavior was investigated [24-26].

The photoluminescence (PL) was investigated by annealing the $\text{Mg}_x\text{Zn}_{1-x}\text{O}/\text{ZnO}$ bi-layer, which tuned the Mg composition [27]. Dual-band $\text{Mg}_x\text{Zn}_{1-x}\text{O}$ UV-PDs were fabricated by employing two $\text{Mg}_x\text{Zn}_{1-x}\text{O}$ layers with different Mg compositions [28]. The Mg atomic reconstruction was observed in p-type interface (ZnO on Zn-polar MgZnO), but not in n-type interface (MgZnO on Zn-polar ZnO) due to the different polarity of the interface [29]. The Mg atomic reconstruction was not caused by thermal diffusion, instead by the asymmetry of energy scales.

In this work, the Mg thermal diffusion behavior on the MSM-PDs with the $\text{Mg}_x\text{Zn}_{1-x}\text{O}/\text{ZnO}$ bi-layer was studied. We found that by increasing the annealing temperature of the $\text{Mg}_x\text{Zn}_{1-x}\text{O}/\text{ZnO}$ bi-layer, one could modulate the detection band of the fabricated MSM-PDs from two bands into one band.

2 Experiments

ZnO and $\text{Mg}_x\text{Zn}_{1-x}\text{O}$ layers with a thickness of 250 nm were deposited consecutively on a sapphire substrate using an RF magnetron sputtering system with a substrate temperature of 200 °C in a 10-mTorr Ar atmosphere. X-ray photoelectron spectroscopy showed the Mg content being 0.3 in the as-deposited $\text{Mg}_x\text{Zn}_{1-x}\text{O}$ film. Then, the $\text{Mg}_x\text{Zn}_{1-x}\text{O}/\text{ZnO}$ bi-layers were annealed at various temperatures between 700 and 900 °C for 2 h, which forced the Mg atom to diffuse from $\text{Mg}_x\text{Zn}_{1-x}\text{O}$ to the underlying ZnO layer. The as-deposited (not annealed) $\text{Mg}_x\text{Zn}_{1-x}\text{O}/\text{ZnO}$ bi-layer was also prepared for comparison. MSM-PDs were fabricated by evaporating Au electrodes on the $\text{Mg}_x\text{Zn}_{1-x}\text{O}$ surface in an interdigitated pattern. Inter-diffusion behavior of Mg atoms was studied by absorption, PL, and secondary ion mass spectrometry (SIMS) measurements. Current–voltage (I – V) characteristics were recorded using a Keithley 2400 source meter, and the photoresponse was measured with a monochromator by illuminating the samples from the $\text{Mg}_x\text{Zn}_{1-x}\text{O}$ side with a 300-W Xe arc lamp.

3 Results and discussions

Dark I – V characteristics of the fabricated MSM-PDs for the as-deposited and various-temperature-annealed $\text{Mg}_x\text{Zn}_{1-x}\text{O}/\text{ZnO}$ bi-layer are shown in Fig. 1. Clearly, the current increases with annealed temperature because the sheet resistance of the $\text{Mg}_x\text{Zn}_{1-x}\text{O}$ and ZnO layers was reduced by the thermal energy of the annealing process. With increasing annealing temperature, the sheet resistance of the ZnO and $\text{Mg}_x\text{Zn}_{1-x}\text{O}$ layers decreased

from $179 \text{ M}\Omega/\square$ and $189 \text{ M}\Omega/\square$ for the as-deposited films to $0.6 \text{ K}\Omega/\square$ and $100 \text{ K}\Omega/\square$ for the ones annealed at 900°C .

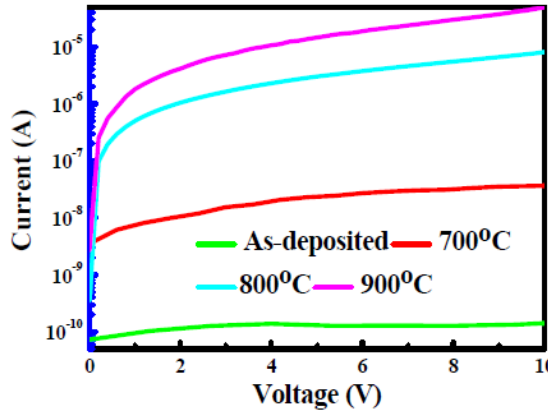


Fig. 1. Dark I - V characteristics of the fabricated MSM-PDs with as-deposited and various-temperature-annealed $\text{Mg}_x\text{Zn}_{1-x}\text{O}/\text{ZnO}$ bi-layer

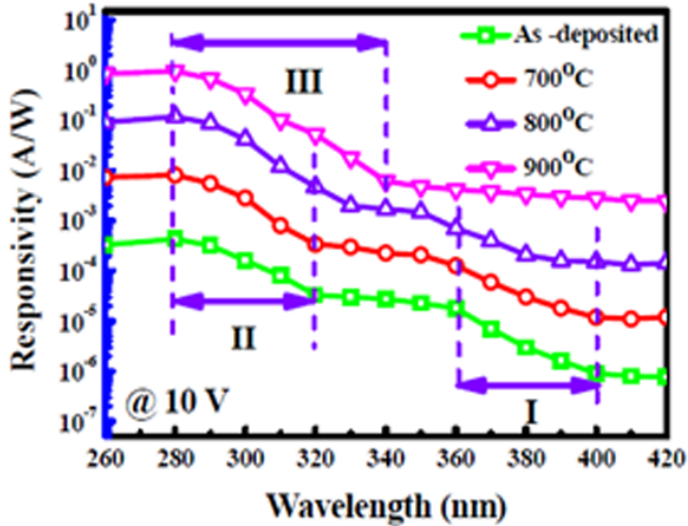


Fig. 2. Responsivity versus wavelengths for the MSM-PDs with as-deposited and various-temperature-annealed $\text{Mg}_x\text{Zn}_{1-x}\text{O}/\text{ZnO}$ bi-layer biased at 10-V voltage

The plot of responsivity versus wavelength for the MSM-PDs with as-deposited and various-temperature-annealed $\text{Mg}_x\text{Zn}_{1-x}\text{O}/\text{ZnO}$ bi-layer biased at 10 V is shown in Fig. 2. It is interesting that the MSM-PDs with as-deposited and 700–800 °C annealed $\text{Mg}_x\text{Zn}_{1-x}\text{O}/\text{ZnO}$ bi-layer demonstrate two sharp increasing bands in responsivity, that is; the MSM-PDs have two detection bands, I and II. In contrast, only one sharp increasing band is observed in the MSM-PDs with 900 °C annealed $\text{Mg}_x\text{Zn}_{1-x}\text{O}/\text{ZnO}$ bi-layer, meaning these MSM-PDs has only one detection band, III.

In the MSM-PDs with as-deposited and 700–800°C annealing, the sharp increasing band of region I, wavelength region of 360–400 nm, originated from the absorption of ZnO layer. However, the sharp increasing band of region II comes from the absorption of the $\text{Mg}_x\text{Zn}_{1-x}\text{O}$ layer, having a wavelength region of 280–320 nm. In contrast, the absorption band of ZnO disappears and only one absorption band is observed in the MSM-PDs with 900 °C

annealed $Mg_xZn_{1-x}O/ZnO$ bi-layer. This absorption band has a wavelength region of 280–340 nm, which is shorter than the absorption region (360–400 nm) of ZnO. Thus, the one absorption band (280–340 nm) is an absorption result of the $Mg_xZn_{1-x}O$ layer with Mg content (x value) less than 0.3 for the as-deposited $Mg_xZn_{1-x}O$ [10,11, 30].

More evidence of Mg inter-diffusion can be observed in the SIMS depth profile of the as-deposited and various temperature annealed $Mg_xZn_{1-x}O/ZnO$ bi-layers, shown in Fig. 3. It is clear that the top $Mg_xZn_{1-x}O$ and bottom ZnO layers are present in the as-deposited $Mg_xZn_{1-x}O/ZnO$ bi-layer with Mg concentration of about 30%, shown in Fig. 3(a). The sharp interface between $Mg_xZn_{1-x}O$ and ZnO leads two detection bands in the MSM-PDs with the as-deposited $Mg_xZn_{1-x}O/ZnO$ bi-layer, shown in Fig. 2. No significant Mg diffusion is seen in the 700 °C annealed $Mg_xZn_{1-x}O/ZnO$ bi-layer, shown in Fig. 3(b), which causes a similar responsivity between the MSM- PDs with as-deposited and 700 °C annealed $Mg_xZn_{1-x}O/ZnO$ bi-layer, also shown in Fig. 2.

Whereas a significant Mg diffusing, from top $Mg_xZn_{1-x}O$ into the underlying ZnO layer, is present in the 800 °C annealed $Mg_xZn_{1-x}O/ZnO$ bi-layer, shown in Fig. 3(c). The Mg diffusion results in decreased Mg concentration from ~30% for the as-deposited (Fig. 3(a)) to ~23% for the 800 °C annealed $Mg_xZn_{1-x}O/ZnO$ bi-layer, shown in Fig. 3(c). The decrease in Mg concentration causes a red-shift of the $Mg_xZn_{1-x}O$ absorption edge; the Mg atom also diffuses into the underlying ZnO layer, generating a blue-shift of the ZnO absorption edge. On further increasing the annealing temperature to 900 °C, the $Mg_xZn_{1-x}O/ZnO$ bi-layer gets homogenized into a single $Mg_xZn_{1-x}O$ layer with ~8% Mg distributed almost uniformly as shown in Fig. 3(d), leading to only one detection band in the 900 °C annealed MSM-PDs, shown in Fig. 2.

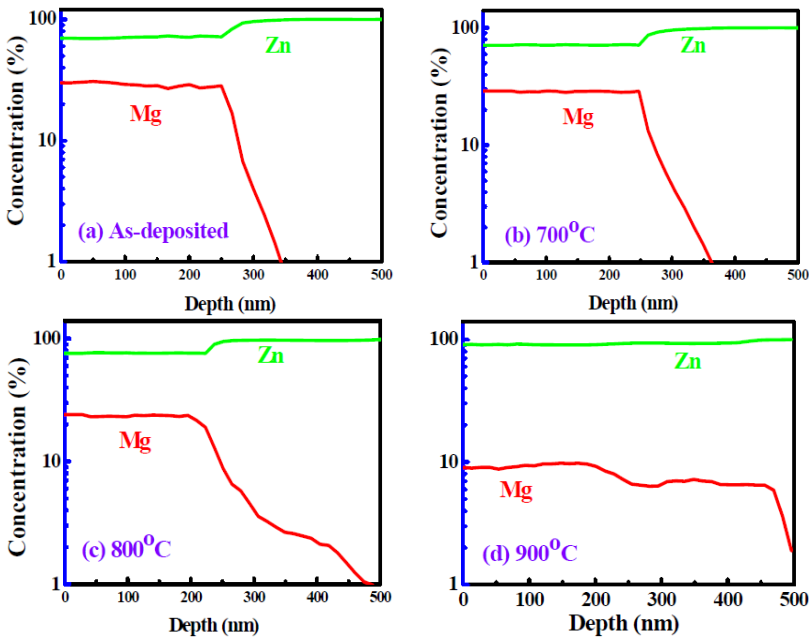


Fig. 3. SIMS depth profile of the as-deposited and various temperature annealed $Mg_xZn_{1-x}O/ZnO$ bi-layer

The normalized PL spectra of the as-deposited and various-temperature-annealed $Mg_xZn_{1-x}O/ZnO$ bi-layer are shown in Fig. 4. The as-deposited $Mg_xZn_{1-x}O/ZnO$ bi-layer

demonstrates two distinct peaks located at about 340 and 400 nm for the emissions of the $Mg_xZn_{1-x}O$ and ZnO layers, respectively, as shown in Fig. 4(a). PL is maintained at almost the same peak wavelengths in the 700 °C annealed $Mg_xZn_{1-x}O/ZnO$ bi-layer, shown in Fig. 4(b). It is a fact that no significant Mg diffusion is observed in the SIMS depth profile of Fig. 4(b). However, compared to the as-deposited $Mg_xZn_{1-x}O/ZnO$ bi-layer, the annealed $Mg_xZn_{1-x}O/ZnO$ bi-layer reveals a larger emission peak in $Mg_xZn_{1-x}O$ than that in ZnO.

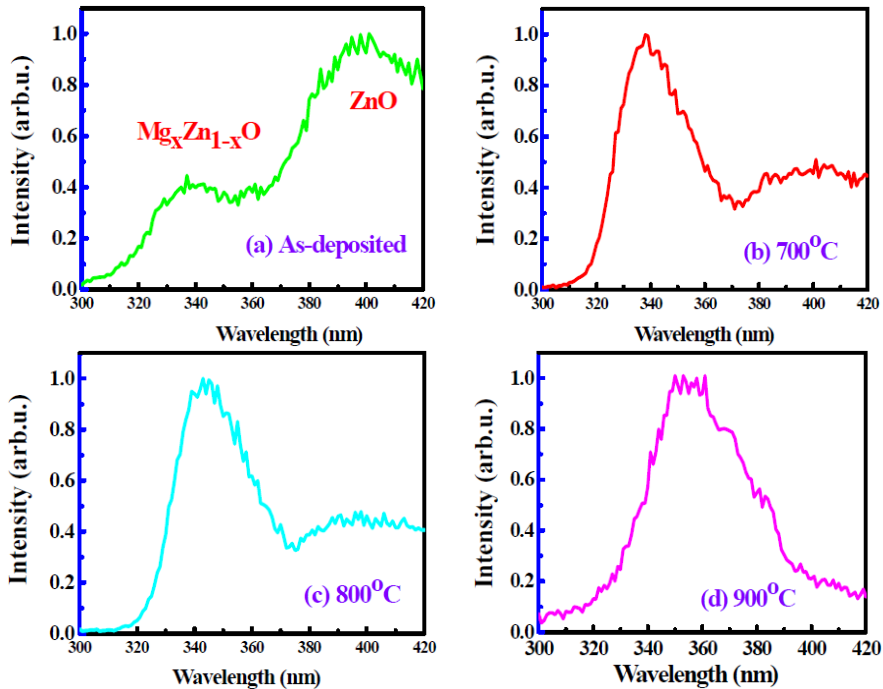


Fig. 4. Normalized PL spectra of the as-deposited and various-temperature-annealed $Mg_xZn_{1-x}O / ZnO$ bi-layer

This is because the crystalline property of the $Mg_xZn_{1-x}O$ film is largely improved after annealing due to the full width at half maximum being drastically reduced from 0.54° to 0.36° for the as-deposited and 700 °C annealed $Mg_xZn_{1-x}O$ layers, respectively. $Mg_xZn_{1-x}O$ is the top layer, and the incident light is illuminated from the $Mg_xZn_{1-x}O$ side in the PL measurement. When raising the annealing temperature to 800°C, the emission wavelength of $Mg_xZn_{1-x}O$ is red-shifted and that of the ZnO is blue-shifted, due to the Mg diffusing across $Mg_xZn_{1-x}O/ZnO$ interface, shown in Fig. 4(c). On further increasing the annealing temperature to 900°C, only one PL peak occurs at about 355 nm, due to the completely homogenized $Mg_xZn_{1-x}O$ layer generated, as shown in Fig. 4(d).

4 Conclusions

The tunable detection band of MSM-PDs with $Mg_xZn_{1-x}O/ZnO$ bi-layer was fabricated. By varying the annealing temperature from 700 to 900 °C during fabrication, we can modulate the detection band of the fabricated MSM-PDs from two bands into one band. When the annealing temperature is lower than 900 °C, two distinct detection bands were

achieved due to the absorption of $Mg_xZn_{1-x}O$ and the underlying ZnO layers. When the annealing temperature was raised to 900 °C, only one detection band was observed in the NSM-PDs. This is because the $Mg_xZn_{1-x}O/ZnO$ bi-layer is completely mixed into one $Mg_xZn_{1-x}O$ layer owing to the diffusion of Mg atoms from $Mg_xZn_{1-x}O$ to the underlying ZnO layer. PL measurement show that there are two emission peaks in the as-deposited and 700–800 °C annealed $Mg_xZn_{1-x}O/ZnO$ bi-layer. However, only one emission peak was found in the 900°C annealed $Mg_xZn_{1-x}O/ZnO$ bi-layer. Equations should be centred and should be numbered with the number on the right-hand side.

Acknowledgement: This work was supported by the Ministry of Science and Technology of the Republic of China, Taiwan, under Contract No. MOST 105-2112-M-415-001-MY3.

References

1. H. Endo, M. Sugibuchi, K. Takahashi, S. Goto, S. Sugimura, K. Hane, Y. Kashiwaba, *Appl. Phys. Lett.* **90**, 121906 (2007)
2. J.D. Hwang, F.H. Wang, C.Y. Kung, M.C. Chan, *IEEE Trans. Nanotechnology* **14**, 318 (2015).
3. G. Cheng, X. Wu, B. Liu, B. Li, X. Zhang, Z. Du, ZnO nanowire Schottky barrier ultraviolet photodetector with high sensitivity and fast recovery speed, *Appl. Phys. Lett.* **99**, 203105 (2011)
4. G. Tabares, A. Hierro, J.M. Ulloa, A. Guzman, E. Muñoz, A. Nakamura, T. Hayashi, J. Temmyo, High responsivity and internal gain mechanisms in Au-ZnMgO Schottky photodiodes, *Appl. Phys. Lett.* **96**, 101112 (2010)
5. J.D. Hwang, J.S. Lin, S.B. Hwang, Annealing effects on MgZnO films and applications in Schottky-barrier photodetectors, *J. Phys. D: Appl. Phys.* **48**, 405103 (2015)
6. Y.K. Su, S.M. Peng, L.W. Ji, C.Z. Wu, W.B. Cheng, C.H. Liu, Ultraviolet ZnO Nanorod Photosensors, *Langmuir* **26**, 603 (2010)
7. S.J. Young, L.W. Ji, S.J. Chang, X.L. Du, ZnO Metal-Semiconductor-Metal Ultraviolet Photodiodes with Au Contacts, *J. Electrochem. Soc.* **154**, H26 (2007)
8. L.K. Wang, Z.G. Ju, J.Y. Zhang, J.D. Zheng, Z. Shen, B. Yao, D.X. Zhao, Z.Z. Zhang, B.H. Li, C.X. Shan, Single-crystalline cubic MgZnO films and their application in deep-ultraviolet optoelectronic devices, *Appl. Phys. Lett.* **95**, 131113 (2009)
9. S. Han, Z. Zhang, J. Zhang, L. Wang, J. Zheng, H. Zhao, Y. Zhang, M. Jiang, S. Wang, D. Zhao, C. Shan, B. Li, D. Shen, Photoconductive gain in solar-blind ultraviolet photodetector based on Mg_{0.52}Zn_{0.48}O thin film, *Appl. Phys. Lett.* **99**, 242105 (2011)
10. L.K. Wang, Z.G. Ju, J.Y. Zhang, J.D. Zheng, Z. Shen, B. Yao, D.X. Zhao, Z.Z. Zhang, B.H. Li, C.X. Shan, *Appl. Phys. Lett.* **95**, 131113 (2009)
11. Q. Zheng, F. Huang, J. Huang, Q. Hu, D. Chen, K. Ding, *IEEE Electron Dev. Lett.* **33**, 1033 (2012).
12. J.D. Hwang, S.Y. Wang, S.B. Hwang, *J. Alloy. compd.* **656**, 618 (2016)
13. J.D. Hwang, J.S. Lin, S.B. Hwang, Annealing effects on MgZnO films and applications in Schottky-barrier photodetectors, *J. Phys. D: Appl. Phys.* **48**, 405103 (2015)
14. Q. Zheng, F. Huang, K. Ding, J. Huang, D. Chen, Z. Zhan, Z. Lin, MgZnO-based metal-semiconductor-metal solar-blind photodetectors on ZnO substrates, *Appl. Phys. Lett.* **98**, 221112 (2011).
15. J.D. Hwang, C.C. Yang, C.M. Chu, MgZnO/ZnO Two-Dimensional Electron Gas Photodetectors Fabricated by RF-Sputtering, *ACS Appl. Mat. Interfaces* **9**, 23904 (2017)
16. T.H. Wu, I.C. Cheng, C.C. Hsu, J.Z. Chen, *J. Alloy. compd.* **628**, 68 (2015)

17. R. Liu, D. Jiang, Q. Duan, L. Sun, C. Tian, Q. Liang, S. Gao, J. Qin, *Appl. Phys. Lett.* **5**, 043505 (2014)
18. J.D. Hwang, G.S. Lin, *Nanotechnology* **27**,375502 (2016)
19. L.K. Wang, Z.G. Ju, J.Y. Zhang, J.D. Zheng, Z. Shen, B. Yao, D.X. Zhao, Z.Z. Zhang, B.H. Li, C.X. Shan, *Appl. Phys. Lett.* **95**, 131113 (2009)
20. Q. Zheng, F. Huang, J. Huang, Q. Hu, D. Chen, K. Ding, *IEEE Electron Dev. Lett.* **33**, 1033 (2012)
21. T.H. Wu, I.C. Cheng, C.C. Hsu, J.Z. Chen, UV photocurrent responses of ZnO and MgZnO/ZnO processed by atmospheric pressure plasma jets, *J. Alloy. compd.* **628**, 68 (2015)
22. R. Liu, D. Jiang, Q. Duan, L. Sun, C. Tian, Q. Liang, S. Gao, J. Qin, Origin of the responsivity characteristics of Au/ZnO/MgZnO and Au/MgZnO/ZnO structured ultraviolet photodetectors, *Appl. Phys. Lett.* **105**, 043505 (2014)
23. J.D. Hwang, G.S. Lin, Single- and dual-wavelength photodetectors with MgZnO/ZnO metal-semiconductor-metal structure by varying the bias voltage, *Nanotechnology* **27**, 375502 (2016)
24. H.A. Chin, I.C. Cheng, C.I. Huang, Y.R. Wu, W.S. Lu, W.L. Lee, J.Z. Chen,; K.C. Chiu, T.S. Lin, Two dimensional electron gases in polycrystalline MgZnO/ZnO heterostructures grown by rf-sputtering process, *J. Appl. Phys.* **108**, 054503 (2010)
25. H. Tampo, H. Shibata, K. Matsubara, A. Yamada, P. Fons, S. Niki, Two-dimensional electron gas in Zn polar ZnMgO/ZnO heterostructures grown by radical sources molecular beam epitaxy, *Appl. Phys. Lett.* **89**, 132113 (2006)
26. M. Brandt, H.V. Wenckstern, G. Benndorf, H. Hochmuth, M. Lorenz, M. Grundmann, Formation of a two-dimensional electron gas in ZnO/MgZnO single heterostructures and quantum wells, *Thin Solid Films* **518**, 1048 (2009)
27. A.K. Das, P. Misra, R.S. Alimsha, A. Bose, S.C. Joshi, S. Porwal, T.K. Sharma, S.M. Oak, L.M. Kukreja, Ultraviolet/visible photodiode of nanostructure Sn-doped ZnO/Si heterojunction, *J. Appl. Phys.* **114**, 183103 (2013)
28. Y.N. Hou, Z.X. Mei, H.L. Liang, D.Q. Ye, C.Z. Gu, X.L. Du, Dual-band MgZnO ultraviolet photodetector integrated with Si, *Appl. Phys. Lett.* **102**, 153510 (2013)
29. K. Imasaka, J. Falson, Y. Kozuka, A. Tsukazaki, M. Kawasaki, Spontaneous polarization driven Mg concentration profile reconstruction in MgZnO/ZnO heterostructures, *Appl. Phys. Lett.* **104**, 242112 (2014)
30. P. Kumar, H. Malik, A. Ghosh, R. Thangavel, K. Asokan, Bandgap tuning in highly c-axis oriented Zn_{1-x}Mg_xO thin films, *Appl. Phys. Lett.* **102**, 221903 (2013)